

Magnestar Inc.
University of Regina

Magnetic Manipulation of Non-Ferrous Metals

Prepared by

Braydon Walker
Nicholas Altwasser

Advised by

Dr. Paul Laforge

April 11th, 2023

Abstract

Small space debris is a growing threat to spacecraft. Due to the size of the debris (<5cm), ground based detection stations are unable to track these objects making traditional collision avoidance methods difficult. Based on a request from Magnestar, a system to remotely manipulate non-ferrous objects was designed to demonstrate the feasibility of moving debris out of the collision path of a spacecraft. Using a ferromagnetic core surrounded by three electromagnets, eddy currents can be induced in non-ferromagnetic debris resulting in a force. By varying the strength of each electromagnet with a custom driver module, the direction and magnitude of the force can be controlled, moving the object out of the collision path with the spacecraft. This test system will aid in developing improved algorithms and electromagnet design for controlling debris manipulation in the future.

TABLE OF CONTENTS

Abstract	
1. Introduction.....	
2. Methodology.....	1
2.1 System	3
Overview.....	3
2.2 Power Supply	4
System.....	5
2.3 Electromagnet	6
System.....	6
2.4 Coil Driver	7
System.....	7
2.4.1 Driver	8
System.....	8
2.4.2 Mosfet	9
Protection.....	9
2.4.3 Controller	10
System.....	10
2.5 Data Logging	12
System.....	12
2.5.1 Power Monitoring	12
Sensor.....	13
2.5.2 Temperature	15
Sensor.....	15
2.5.3 Magnetic Flux	15
Sensor.....	15
2.5.4 Camera	16
Tracking.....	16
2.5.5 User Interface & Log	17
Files.....	18
2.5.6 Communication to Coil	20
Driver.....	20
2.6	21
Coding.....	21
2.6.1 Coil Driver System	22
Coding.....	23
2.6.2 Data Logging System	
Coding.....	

3. Testing & Findings.....	
.....	
3.1 Electromagnet System.....	
3.2 Coil Driver System Testing.....	
3.3 Data Logging System Testing.....	
3.3.1 Current Measuring Testing.....	
3.3.2 Voltage Measuring Testing.....	
3.3.3 Temperature Sensor Testing.....	
3.4 Final System Testing.....	
....	
3.4.1 Magnetic Flux Density Results.....	
3.4.2 Object Manipulation Results.....	
3.5 Specifications.....	
.....	
4. Conclusion.....	
.....	
5. Future Recommendations.....	
.....	
5.1 Wider Variety of Testing.....	
5.2 Real-Time Systems.....	
.....	
5.3 Environmental Energy Capture.....	
6. References.....	
.....	
7. Appendices.....	
.....	

1. Introduction

The device developed for Magnestar consisted of four main subsystems with the combined goal of creating a rotating dipole that would be manipulated to induce eddy currents into non-ferrous metals in the immediate surroundings. The device would then continue manipulating its created magnetic field to interfere with the magnetic field created by the eddy currents on the non-ferrous object to induce torques and, ultimately, forces on the non-ferrous metal. This approach has been previously proven to work successfully by a research group based out of the University of Utah (Pham et al., 2021). The main objective was to assess the feasibility of using this device in a space based setting. The device would manipulate and deflect damaging debris that could collide with spacecraft, rendering them harmless and preventing damage to spacecraft. By doing so, the aim was to enhance the safety and longevity of space missions.

2. Methodology

2.1 System Overview

The project as a whole would run on 120VAC, which can easily be altered to run off of the power system in a spacecraft with modifications to the power system and without any modifications to other systems. The project comprises four main subsystems. The power supply system, which supplies power to the other subsystems and to the coil drivers to drive the electromagnet coils. The coil driver circuits, which convert 12VDC to a sine wave with variable frequency, phase, and amplitude to send to each of the three electromagnet coils. The electromagnet system would receive the sine wave from the coil drivers and have it run through the electromagnets themselves. The final system, the data logging system, consists of various sensors to monitor the system and its outputs, and provides a user interface for testing purposes.

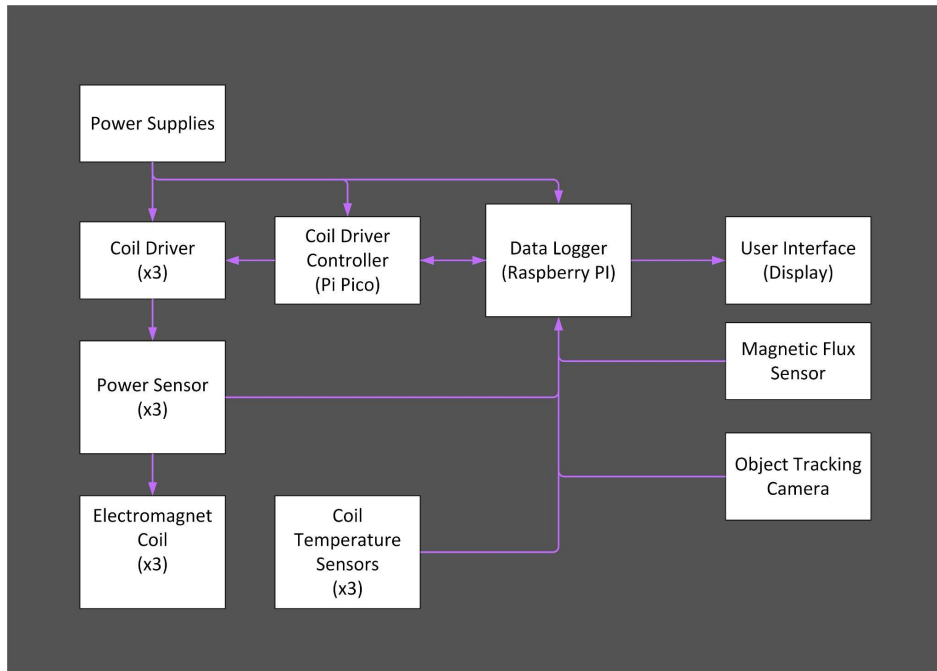


Figure 1: System Overview Block Diagram

2.2 Power Supply System

The power supply system provides power to the coil drivers, coil driver controller and data logging processor. The system comprises a 12 volt system for the coil drivers and a 5 volt system for the coil driver controller and the data logging processor. The 12 volt system uses two Mornsun LM20B-12 switch mode power supplies, each capable of outputting 102 watts (Mornsun, 2022), which are paralleled to provide a total of 204 watts. The coil driver system was originally designed to use a half bridge to generate an AC waveform, which required a dedicated positive and negative supply. However, the design was later changed to an H-bridge configuration, which will be discussed at a later point. To accommodate this change, two lower wattage power supplies were used instead of a single higher wattage power supply as originally anticipated. The 5 volt system is powered by a Mornsun LM25-23B05 switch mode power supply capable of outputting 25 watts (Mornsun, 2021). All three power supplies 120 VAC connections are tied together using distribution blocks, enabling the system to be powered on using a single 120 VAC wall plug. The specifications for the power supply system are to provide 12V DC +/- 2.5%, 10A +/- 2.5% and 5 VDC +/- 2.5%, 5A +/- 2.5% (Note: the original specification for the 5 VDC is to supply current of 10A, but this was sized for using three Pi Pico's and a Raspberry Pi 4. The as-built system only uses one Pi Pico and Raspberry Pi 4. This spec has been reduced to 5A).

2.3 Electromagnet System

The electromagnet system consisted of a 3D printed frame of abs for the benefit of having a higher heat deflection temperature compared to PETG or PLA filament. The heat deflection of ABS provided a large advantage being 100 C, when compared to PLA and PETG. PETG had other downsides as well, other than the heat deflection temperature. In Figure 1, the comparison of the heat deflection temperatures of the filaments that were considered for the frame design can be examined.

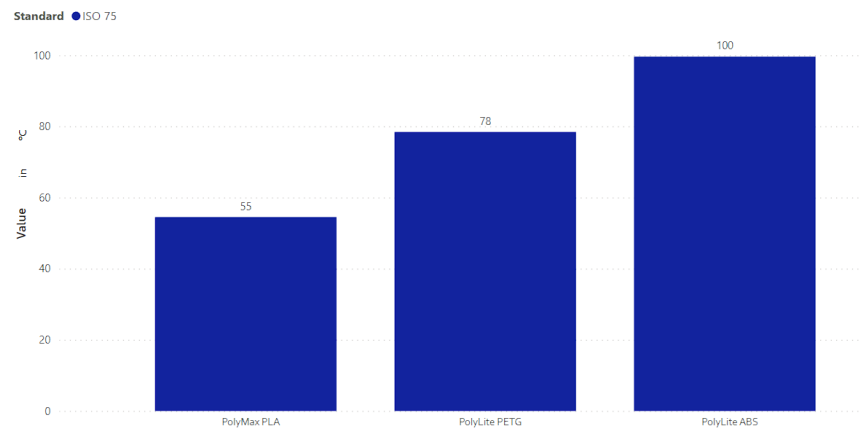


Figure 1: Heat deflection temperatures of PETG, PLA and ABS
Source: (Polymaker, 2023)

The frame design was inspired by the frame design of the University of Utah research group (Pertruska, 2014, f. 3). Modifications were made to the frame to allow simple and toolless disassembly of the electromagnet system so swapping the core out would be a simple task that would allow easier comparison of the effects of different core shapes and material to be used in the system. Each frame is designed to sit tightly over top of the frame/core inside of itself to allow the electromagnet coils to be as close to the core as possible. The frame sizes for each electromagnet coil ended up being 86.8 mm, 120.8 mm and 158 mm cubed for the inner, middle and outer electromagnet coil, respectively. A cubic core with a side length of 50.8mm was used as the focal point for our magnetic dipole to concentrate.

The three coils used in the electromagnet system were each wrapped using 16 AWG magnet wire with an ampacity of 11 Amps at 75 C (Blue Sea Systems, 2023). The inner coil was wrapped 350 times with six layers to achieve a peak Ampturn output of 1750. The middle coil was wrapped 412 times with five layers to achieve a peak Ampturn output of 1318. The outer

electromagnet coil was wrapped 409 times with four layers to reach a peak Ampturn output of 1104. In Figure 2, the final electromagnet configuration can be viewed.

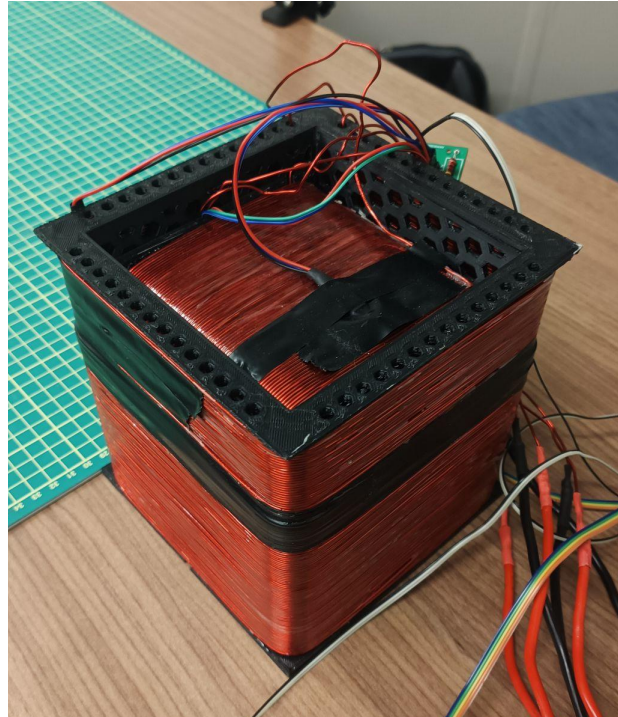


Figure 2: Nested Electromagnet System with temperature wires and leads connected

2.4 Coil Driver System

The coil driver system consisted of two separate subsystems. The first is the controller system, which consists of a Raspberry Pi Pico H. The second system is the driver system, an h-bridge circuit that is switched by the controller system to allow current to flow both forwards and backwards through the electromagnet coils.

2.4.1 Driver System

The driver system consists of three circuits built on custom design PCB's, one for each electromagnet coil, designed from an h-bridge design with multiple mosfet protection schemes added. The PCB's use exposed traces 2.5mm in width to allow enough heat dissipation to not damage the board according to IPC-2221 standards. The driver system takes pulse width modulation and GPIO signals from the controller system to activate the driver circuit's high and low, positive and negative gates individually to create sine waves. These sine waves are then fed to the electromagnet system. The h-bridge uses STDP6F6 p-channel mosfets as the highside switches. These mosfets are being switched by AOT2618L n-channel mosfets to allow us to control p-channel fets with a positive input. The design to control the p-channel mosfets with a

positive signal was provided by Douglas Wagner a professor at the University of Regina Engineering Department (Wagner, 2023). The h-bridge also uses STDP6F6 n-channel mosfets as lowside switches. It was found that our inner electromagnet coil was drawing more current than expected so we had to add heatsinks to our STDP6F6 p-channel mosfets to allow for adequate heat dissipation.

2.4.2 Mosfet Protection

The driver systems have multiple layers of protection added for the mosfets to try to eliminate the inductive flyback experienced from switching an inductive load. Two schottky diodes are connected from each side of the coil to the positive supply rail, and two schottky diodes are connected from the ground rail to each side of the coil. These diodes are placed here so that when inductive flyback is experienced, they go through these diodes instead of the mosfet's diodes. There is a 1mF decoupling capacitor across the terminals of the positive and ground to absorb excess voltage created by the inductive flyback. An RC snubber circuit is attached in parallel to the electromagnet coils to absorb this excess voltage from the inductive flyback. It is sized with a 220uF capacitor and 3.9ohm resistor. The final form of protection used is a TVS diode placed across the terminals of the electromagnet coil. This diode only activates when the voltage is greater than 12.7V when it starts allowing current to pass through itself, causing none of the voltage to be applied to our driver system.

2.4.3 Controller System

The controller system takes data from the data logging system using the UART data transfer protocol and UART class from the machine micropython library (George & Sokolovsky, 2023). The data being brought into the system can be in three forms. The first is a simple stop command which immediately turns off the output from the driver system. The second form is a simple start command which starts the outputs to the electromagnet. The third is a command with the object's position and the object's wanted position. The system calculates the required sine waves to induce the desired force on the object by applying a set of known constants and input data through mathematical computations. This resulting sine wave is then modified into a table of pulse width modulation values to be used to control the driver system. The controller system uses multi-threading to be able to do the above tasks simultaneously while constantly cycling through the tables of sine wave values sending pulse width modulation schemes to the mosfets in the driver system (George & Sokolovsky, 2023). The controller system uses the micropython machine library's pin, pwm and gpio classes to achieve the ability to control pins and outputs on the Raspberry Pi Pico.

2.5 Data Logging System

The data logging system takes in data from three power monitoring sensors, three temperature sensors, one 3D hall effect sensor and a Camera. The goal of this system is to provide the operator with the ability to start and stop tests, provide a live view of all the sensors while a test is ongoing and store the captured data for further analysis. The sensor data is taken using a Raspberry Pi 4B. The information is displayed in a live user interface and stored in csv log files to review after a test has been completed. The specification for the data logging system is to take in measurements from all sensors every 100 milliseconds.

2.5.1 Power Monitoring Sensor

The power monitoring sensor used is an Allegro ACS37800 that reports current and voltage output from the coil driver circuit. While the voltage information is convenient to have, the current is important to monitor, as when captured, it can be overlaid with the measured magnetic flux density to find the currents that produce the strongest magnetic flux density. The sensor has a specified accuracy for voltage measurements of $\pm 1\%$ and for current of $\pm 2\%$ (Microsystems, 2022). A PCB was designed to mount the sensor on to. The voltage measurement circuit was followed from the data sheet. Due to the potential for large currents to be flowing through the PCB, IPC-2221 (IPC, 2003) was followed to determine the minimum allowable trace width for a 15 C temperature rise of the PCB high current carrying traces. It was found that for exposed traces, the minimum trace width had to be 5.624mm in diameter for a 1OZ copper board. The minimum trace width on the designed board was selected to be 7.5mm. Since the PCB is a two layer board, the high current traces were mirrored onto the second layer and connected with vias to further mitigate any temperature increases. The circuit design for the voltage measurement part of the circuit was followed from the data sheet to provide the proper isolation requirements (Microsystems, 2022). The sensor uses I2C to communicate with the data logging processor. The PCB was designed to have two pins for each I2C line allowing for the PCB communication lines to be daisy chained together.

2.5.2 Temperature Sensor

Most of the energy supplied to the electromagnet is converted into heat due to the resistance of the electromagnet. This may lead to the ABS frames supporting the electromagnet coils to reach their maximum heat deflection of 100 C, which is a concern for the long-term reliability of the system. To address this issue, temperature sensors are placed on each coil to monitor the coil temperature and ensure the heat deflection temperature of the coil frames is not exceeded. The sensors used are MAX31820 from Maxim Integrated (Maxim Integrated,

2013), which communicate with the data logging processor via Onewire. The sensors have a temperature sensing range of -55c to 125c with an accuracy of $\pm 2^\circ\text{C}$ (Maxim Integrated, 2013), which is in line with the specifications outlined for the temperature sensors measuring coil temperature 0c to 125c with $\pm 2^\circ\text{C}$ of error. By monitoring the temperature of the coils, damage to the system can be prevented and the longevity of the electromagnet enhanced.

2.5.3 Magnetic Flux Sensor

To measure the rotation and magnitude of the dipole generated by the electromagnet, a 3D Hall effect sensor was chosen to provide an independent reading on the x, y and z-axis. The Magnetic Flux Density sensor selected was a Texas Instruments TMAG5273 (Texas Instruments, 2021). The sensor has an accuracy of $\pm 5\%$ with a full range of $\pm 133\text{mT}$ (Texas Instruments, 2021). The sensor uses I2C to communicate with the data logging processor. A PCB was designed to mount the sensor using the typical circuit diagram in the datasheet as a general guide (Texas Instruments, 2021). The specification for this sensor is to provide a reading of the magnetic flux with an accuracy of $\pm 6\text{ mT}$.

2.5.4 Camera Tracking

The Camera Tracking system uses a USB camera connected to the data logging processor. The camera is calibrated to remove any lens distortion to obtain a flat image which real world measurements can be taken from. The camera was calibrated using a combination of codes from Geeks for Geek (2023) and Eser (2020). The camera looks at a green matt with 1cm grid lines with a total size of 58cm x 43cm. The camera is framed such that only the matted surface is visible in the image relating to an image size of 58cm x 43cm. Using Opencv on the image and color masks to filter for desired object color, a new image can be created showing only the object (Opencv, 2022). Taking the center of the object gives the object location in pixel coordinates. Taking the pixel coordinates and relating them to the known image size gives the real world location of the object on the green matt. The specification specific to the camera tracking is to track an object with an accuracy of $\pm 1\text{ cm}$ in both the X and Y coordinates.

2.5.5 User Interface and Log Files

The user interface displays the status of the sensors while tests are running and provides functionality to start and stop tests. It also allows input of values such as the Maximum Allowable Coil Temperature and set points to move the manipulated object to a desired location. Without the need to modify any source code. If the stop button is pressed or a coil temperature sensor exceeds the specified maximum allowable coil temperature, data capture is ceased. All the data taken in by the Data Logging Processor is displayed in graphical form in the interface.

The interface was coded in Python using Kivy (*Kivy, 2011*). Kivy assists in the creation of an application that has buttons, text inputs and graphs. Due to the processing overhead required to draw each plot and write to the csv files, the plots and csv files are not able to update in realtime. Instead, the data from the sensors is buffered until roughly one second worth of data is stored, and then the graph and csv files are bulk updated. The graphs only show the 100 most recent data points. However, every data point taken in by the data logging processor is written to the csv files, so none of the data is lost. One hundred displayed data points on each graph were chosen as it provides a nice balance of the amount of information displayed and the readability of the plot.

2.5.6 Communication to Coil Driver

To communicate with the coil driver processor UART is used from the pyserial library (Pyserial, 2021). Four different commands are sent to the coil driver: start, stop, desired object location and current object location. Before the start of each test, a desired object location is sent, followed by a start command. While the test is running, the current object location is sent to the coil driver processor each time the data logging processor receives a new update from the camera. When the operator presses the stop button or a coil temperature sensor exceeds the maximum allowable temperature, a stop command is sent to the coil driver processor.

2.6 Coding

2.6.1 Coil Driver System Coding

The coil driver system uses multi-threading to be able to run two main functions concurrently (George & Sokolovsky, 2023). The first thread handles communication and calculations. It uses UART to communicate with the data logging system. If the thread receives the stop or stop command, it sends this command to the other thread. If this thread receives a message with two coordinates, the first being the current position of the object and the second being the wanted position of the object, it starts doing calculations. It uses both the coordinates as well as known constants specific to the electromagnet coil such as the number of turns in each electromagnet coil, average number of turns and the radius of the electromagnet coils. It guesses initially the required current, then iterates updating the current guesses until it is able to come to a convergence within a specified tolerance. Once current values are calculated they are sent to the other thread.

The second thread is responsible for controlling the driver system. It initializes the necessary outputs and creates the coil classes. Once complete, it enters a loop through running

the code to continuously control the driver system. At the start, it checks for a kill command. If a kill command has been received, it shuts off the coils by turning on the PMW channels, converting them to GPIO pins, and setting them to output 0V before terminating the program. Next, the thread checks for new data from the first thread. If new data is available, it computes the required percent changes in current from each coil's maximum to accurately scale the look up tables. It then updated the values in the lookup table for each coil. Finally, the thread cycles through the lookup table pulsing each of the values in the tables through pulse width modulation once for each coil, then it delays the next iteration for 1625us, which creates a 15 hz waveform. This cycle repeats indefinitely until a stop command is received by the Pi Pico. The thread has ten main states that it cycles through, which are depicted in Figure 3.

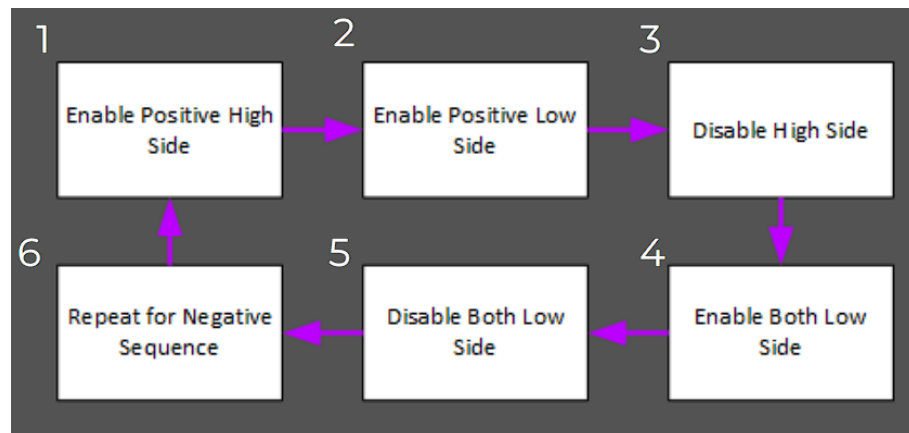


Figure 3: State Diagram of thread two's states

In state 1, the high side enable is achieved simply by setting a gpio pin high. For state 2, the low side enable is determined by the pulse width modulation output from the lookup tables for the sine waves. State 3 and 4 are very crucial in mitigating inductive flyback from the electromagnet coil. Disabling the high side mosfets cuts off power to the coil, while enabling both low sides as gpio high outputs allows the coil to drain any inductive flyback voltage it creates to ground dissipating the excess energy (Duguid, 2023). It is important to note that a delay greater than ten-thousands times the fall of the mosfets is included between each state change. This is to ensure they are fully disabled before proceeding to the next state, which minimizes the risk of a short circuit that could possibly damage the system by causing mosfet failure or power supply trips.

2.6.2 Data Logging System Coding

The data logging system uses multiprocessing (cite) to intake data from each of the sensors while also outputting the data to log files, updating graphs and sending the current object position to the coil driver controller. Multiprocessing was chosen instead of threading as multiprocessing starts each new process in a different instance of Python, allowing for the entire usage of the cpu simultaneously (The Python Software Foundation, 2023). Each sensor type is split into an individual process and starts when the user presses the start button. The system runs continuously until the maximum allowable coil temperature is reached or the user presses the stop button. At this point, all the processes are terminated, and the data intake is stopped. The data logging system code flow is summarized in Appendix B.

3. Testing & Findings

3.1 Electromagnet System

The electromagnet system was tested to find the impedances of each of the electromagnet coils with different cores. This was done using a LCR measurement tool, a Sencore LC-102 tool and using hand calculations. The found values for the inductance of each coil with the different core configurations can be seen in table 1 below.

Type of Measurement	Inner Coil	Middle Coil	Outer Coil
Sencore LC-102	6.5mH	14.4mH	19.8mH
LCR 880	4.98mH	14.68mH	18.5mH
Zcoil	1.63-j0.65 ohms	2.58-j1.4 ohms	3.50-j1.81 ohms
Calculation	6.88mH	14.86mH	19.25mH
Average	6.12mH	14.65mH	19.18mH

Table 1: Coil impedances with no core

Type of Measurement	Inner Coil	Middle Coil	Outer Coil
Sencore LC-102	7.6mH	15.1mH	20.3mH
LCR 880	10.4mH	14.0mH	21.2mH
Zcoil	2.54-j1.37 ohms	2.72-j1.69 ohms	3.54-j1.93 ohms
Calculation	14.54mH	17.9mH	20.04mH
Average	10.85mH	15.67mH	20.51mH

Table 2: Coil impedances with cube core

Type of Measurement	Inner Coil	Middle Coil	Outer Coil
Sencore LC-102	7.17mH	15.06mH	20.2mH
LCR 880	9.825mH	17.06mH	19.74mH
Zcoil	2.48-j1.08 ohms	2.921-j1.40 ohms	3.20-j1.71 ohms
Calculation	11.4mH	14.88mH	18.14mH
Average	9.47mH	15.67mH	19.36mH

Table 3: Coil impedances with cylindrical core

3.2 Coil Driver System Testing

Coil driver testing consisted of testing the pulse width modulation output of the driver system. This was to verify that the overlaps that needed to occur for the mosfets to completely turn off between states were timed properly and were not overlapping incorrectly. If they were this would cause our driver system to short circuit which would destroy mosfets. Testing to verify the change of amplitude, frequency and phase of the three sine waves. This was a simple change of the input and a check on the oscilloscope to see if it had changed as desired. These tests were all completed successfully. The results of one channel of the driver system can be seen in figure 4. The results in figure 4 also show how an ideal lowpass filter could be used to achieve a sine wave as shown in white. It was found later that this was unneeded from the inductance of the electromagnet coil filtering the current waveform adequately.

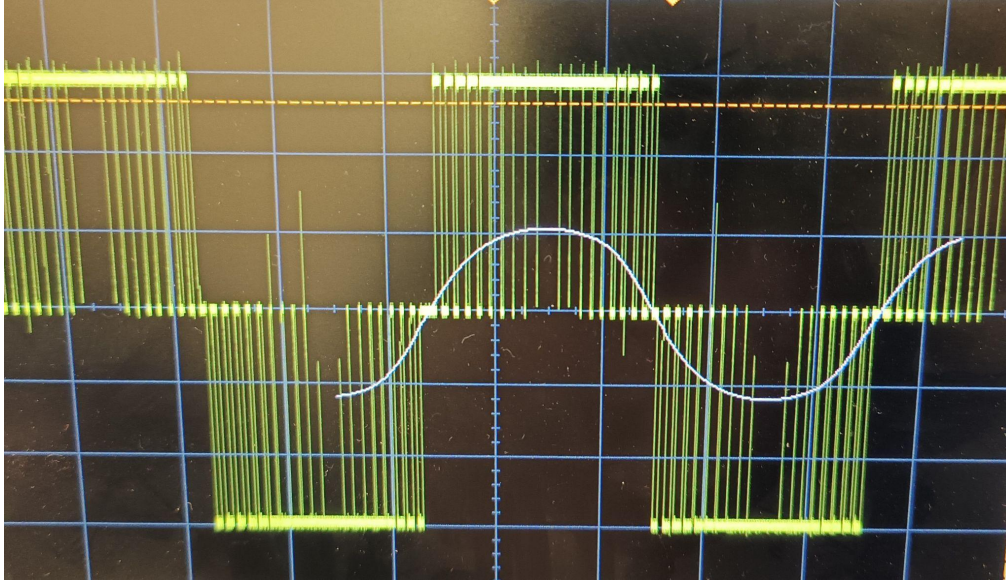


Figure 4: Coil driver system output waveform with resistive load with ideal filter, filtering to result in a 15 Hz sine wave

After the verification of the coil driver function was complete it was hooked up to the system where the waveform could be applied to the electromagnet coils. This allowed us to see how exactly the electromagnet coils were filtering the system as well as if the protection schemes were preventing inductive flyback. The results of this testing can be seen in figure 5. We can see that a relatively accurate sine wave of current is created. It was at this point we realized that voltage doesn't technically matter in our system, because it's the current that creates the magnetic fields.

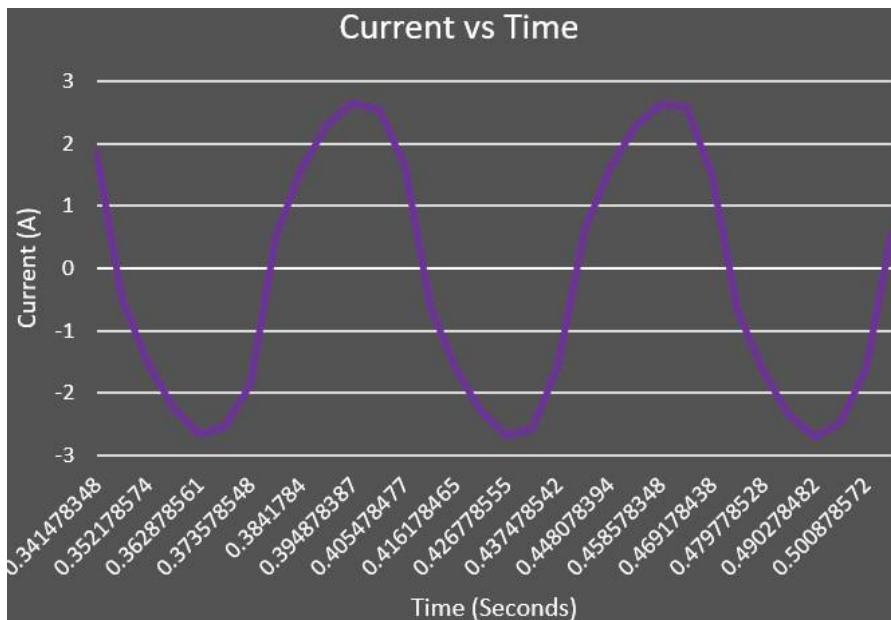


Figure 5: Current output of middle coil driver with inductive load (middle coil)

3.3 Data Logging System Testing

3.3.1 Current Measuring Testing

	Current Expected	Current Measured
Coil Inner	1.5 A	1.28 A
Coil Middle	1.5 A	1.28 A
Coil Outer	1.5 A	1.29 A

Table 4: Expected Current vs Measured Current (DC)

3.3.2 Voltage Measuring Testing

	Voltage Expected	Voltage Measured
Coil Inner	11 V	11.28
Coil Middle	11 V	11.30
Coil Outer	11 V	11.34

Table 5: Expected Voltage vs Measured Voltage (AC)

3.3.3 Temperature Sensor Testing

Testing was done to ensure the temperature sensors provided a reasonably accurate reading while inside a magnetic field. The sensor that is used to verify is an infrared temperature sensor. The temperature of the Inner Coil is not recorded as this test was done in the nested configuration and thus the temperature is unable to be measured with the IR sensor.

Current (A)	Coil Temp Middle (C)	Coil Temp Outer (C)	Coil Temp Middle IR (C)	Coil Temp Outer IR (C)
3 A	20	20.4	19.6	19.9
7A	22.5	21.5	22.6	21.5
8A	23.5	21	24.8	23.1
9A	25	23	26.2	24.2
10A	32	25	32.9	27.9

Table 6: Temperature Sensor Verification

3.4 Final System Testing

After the verification of the functions of each of the subsystems in the project. Testing was done on the system itself to begin characterizing the electromagnetic capabilities of the system.

3.4.1 Magnetic Flux Density Testing

Testing was completed while applying max current to each coil and measuring the magnetic flux density beside the electromagnet system in the range of 0-7 cm from the sides of the electromagnet system. Three measurement graphs are shown below showing the drop off of the magnetic flux density drop offs with distance from the electromagnet system. Figure 6 shows the inner electromagnet coil's direction of magnetic flux. Figure 7 shows the middle electromagnet coil's direction of magnetic flux. Figure 8 shows the outer electromagnet coil's direction of magnetic flux.

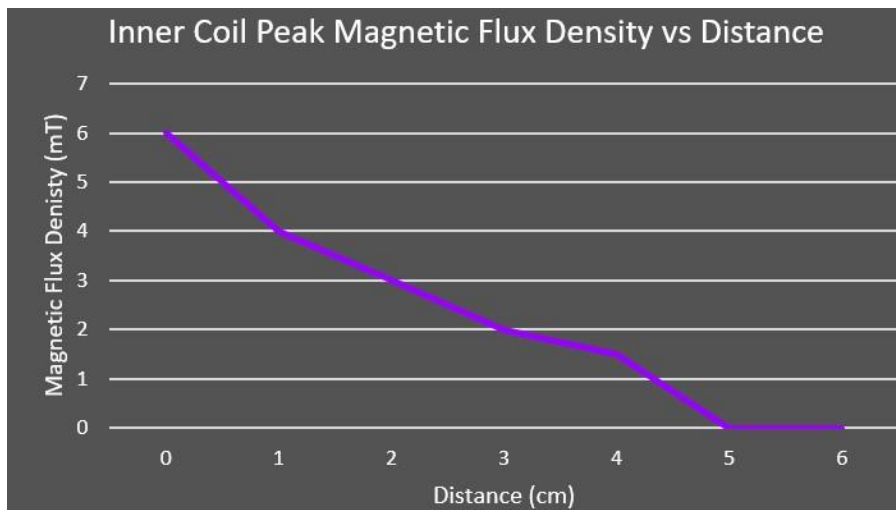


Figure 6: Inner electromagnet coil magnetic flux density drop of with distance

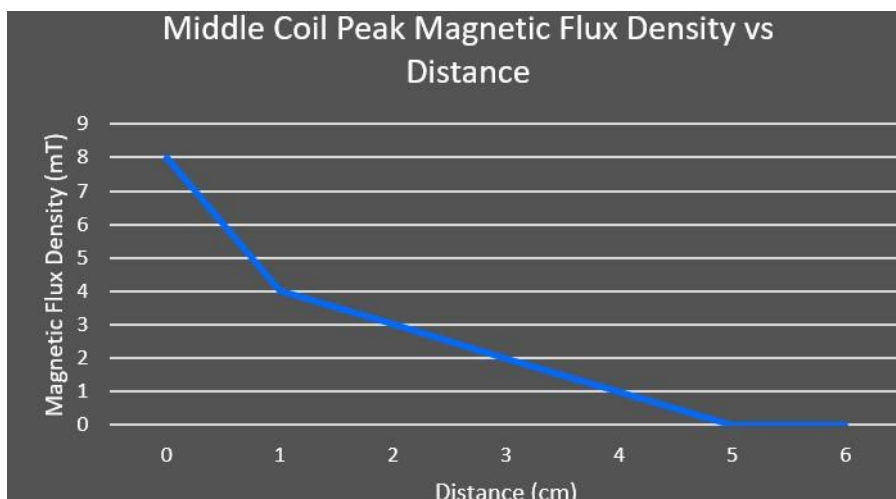


Figure 7: middle electromagnet coil magnetic flux density drop of with distance

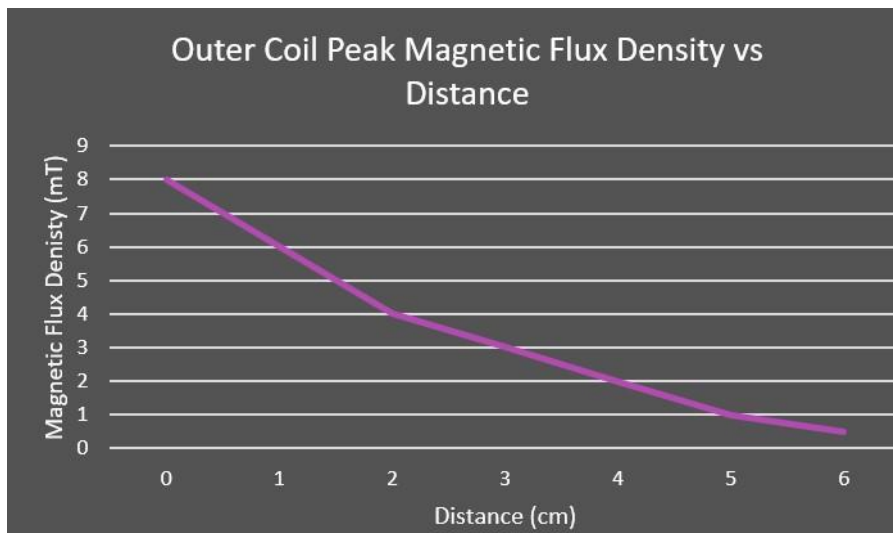


Figure 8: Outer electromagnet coil magnetic flux density drop of with distance

3.4.2 Object Manipulation Results

Testing was completed to look into how this system affected various different ball materials. During tests with non-ferrous metals, we observed no ability to alter the path of or induce movement into these balls. Overcoming the frictional forces experienced at stand still proved to be a big challenge during the testing. Testing was then completed on ferrous metal balls. Slight observations were made to changes in direction and speed of a rolling ball. The system was still unable to move a ferrous ball from standstill proving that frictional forces were causing big issues to the system, limiting repeatability of the experiments with identical inputs. The final testing that was done for the forces induced by the system was with a magnetic tipped screwdriver. It was observed that the screw driver would vibrate slightly while slowly rotating itself to align with the coil's magnetic field line with the strongest magnetic flux densities. This would result in either the screwdriver being rotated towards or away from the electromagnet system depending on the direction of the created magnetic field lines. This observation would not occur at distances greater than 5 cm from the edge of the electromagnet system.

3.5 Specifications

This project's initial specifications included:

- Power supply DC +12V $\pm 2.5\%$ 10A $\pm 2.5\%$
- Power supply DC 5V $\pm 2.5\%$ 10A $\pm 2.5\%$
- Measure movement in 20cm x 20cm area ± 1 cm of fidelity and 2 DOF
- Measure temperature of coils with 0-125c ± 2 c
- Measure magnetic field strength at a distance of 10cm with X ± 0.006 T
- Coil drivers 15 ± 0.5 Hz, Voltage ± 0.1 v, Current ± 0.1 A
- Take measurements every 0.1 seconds
- 16 AWG magnet wire coils with ~ 400 wraps/coil with 3-4 amps of current resulting in 1200-1600 amp turns per coil of peak output
- Mild steel (high iron content) cylindrical core with 2in diameter and height
- Removable brackets to hold the coils to allow the, to be removable, 3d printing with ABS

The power supply specifications have been met for the 12V power supply by using dual LM100-20B12 power supplies to supply 12V DC $\pm 1\%$ with a total current rating of 17A (*Mornsun, 2022*). The 5V power supply specification was originally specified for 3 Raspberry Pi Picos and a Raspberry Pi 4 which we ended up only using 1 pi pico which lowered our current requirement. This specification has been changed to be 5A. This has then been achieved by using a LM25-23B05 power supply, supplying 5V $\pm 2\%$ with a current of 5A, fully meeting the revised specification.

The movement measurement specification was met partially with the trackable area being 58cm x 43cm, the fidelity of ± 1 cm was not met because the tracked object in the system was reflective and therefore would pick up environmental light from its surroundings. This would cause dynamic changes in the color of the ball that did not match the color mask applied using opencv. This would result in the tracking to inaccurately detect the center of the ball. With the ball being 2.6cm in diameter it results in an actual fidelity of ± 3 cm.

The measurement interval specification was met except for the coil temperature sensors. This is because realistically the temperature of the coils is not able to change significantly in 1s of time so the sample rate of the temperature sensors is 1Hz, while the other sensors measure at or faster than 10Hz.

The specifications for the field strength sensor are sampling 10Hz with an accuracy of ± 6 mT. Using a formula specified in the datasheet to calculate the total output error an estimation of the true accuracy of the sensor can be obtained (Texas Instruments, 2021). At a

maximum theoretical value of $\pm 41\text{mT}$ for the electromagnet coils this sensor provides an output error of $\pm 2.05\text{mT}$ this exceeds the spec outlined for measuring the magnetic field of $\pm 6\text{mT}$. Targeting a dipole rotation of 15 Hz reading the sensor at least every 33ms meets the Nyquist criteria for sampling to obtain an accurate representation of the dipole generated. Exceeding the original spec of 10Hz.

The target specification for this system was to sample the voltage and current every 10 Hz. Using the frequency of the sine wave generated by the coil drivers (15 Hz) each sensor needs to be sampled at a rate of 33ms to achieve Nyquist. Which is far faster than the 10 Hz sampling outlined in the specifications. Looking at the data point times in Figure 5 the sampling frequency of the power monitoring sensors is well above the Nyquist sampling criteria. Testing as seen in table 4 and table 5 revealed that the voltage and current measurements report a maximum error of 340mV and 320mA to a known source. Using the offset trim and gain trim registers in the power monitoring sensor the current can be reasonably brought within an accuracy of $\pm 100\text{mA}$. The voltage measurement Rsense ratio can be adjusted to bring the voltage measurement to within an accuracy of $\pm 100\text{mV}$. Another deficiency is when the system is fully integrated the power monitoring sensor is only able to a $\frac{1}{2}$ cycle of the voltage waveform. Since the coil drivers are an H-bridge the Allegro is only able to measure the positive half of the voltage waveform. This is due to the requirement that the Allegro neutral voltage measurement pin must be connected to the device GND of the Allegro. If the coil drives were a half bridge this would not be an issue as the negative supply and positive supply would provide both the positive and negative half of the waveform in reference to ground.

The physical design specifications have been partially met with the electromagnet coils being wrapped in 16 AWG magnet wire. The 400 wraps per electromagnet coil has been met for the middle and outer coil, but the inner coil was unable to fit due to the nested coil configuration. A high iron content mild steel AISI-1018 core was used in this system. The electromagnet system was also designed with ABS 3D printed coils that allow simple and toolless deconstruction.

4. Conclusion

Due to limitations and ultimately the immense challenges of this concept, it is unlikely that this system would be able to be implemented successfully in a space setting and with the purpose of manipulating debris from spacecraft's orbits. This system would have to be scaled approximately ten times in power to have similar results to those in the University of Utah research group's paper (Pertruska, 2014, f. 3). This is a challenge in space where power budgets are extremely tight. This also would not be likely to manipulate objects at a far enough range fast enough to deflect them from a spacecraft's orbital path due to the slightly inverse square result factor of distance that affected the systems magnetic flux density output. With magnetic fields seen in the Utah group's research being around 45mT (Pertruska, 2014, f. 3) and the need to manipulate objects at a distance much greater than centimeters away from the system, it is known that large scaling will need to be done with both the electromagnet system and power system. These options are not likely viable because of the limited energy sources in space and the cost increases that would occur with scaling the electromagnet system as its weight being currently around 11lbs and scaling would just make the cost of sending the system to space ridiculous.

This system itself should be looked at as the start of the research required to develop a system that would be able to complete the objectives. Looking into doing more testing and likely implementing a design that uses beam focusing to focus the magnetic field at the object it is trying to manipulate.

5. Future Recommendations

5.1 Wider Variety of Testing

In the future more testing with

- a larger variety of core shapes and materials will need to be completed to see if a more efficient shape and/or material can be used
- a larger variety of objects and materials to manipulate will need to be completed to see how the system works with objects other than spheres, this will also better characterize the electromagnetic capabilities of the system
- a zero gravity environment, or replica to mimic zero gravity effects on forces to further characterize the magnet in space

5.2 Real-Time Systems

- A real-time system to handle tracking and identifying objects at far distances, with the possibility to identify object shape and size and if possible object material to help feed the coil driver system accurate data.
- A real-time feedback loop of output current, voltage, phase, frequency, object movement, and magnetic dipole strength to feedback to the coil driver to adjust settings to make up for environmental disturbances or unaccounted for parameters.

5.3 Environmental Energy Capture

- While the system was not powered up, the coils would pick up voltage from the forms of RF noise and electromagnetic noise, resulting in a voltage of anywhere from 400mV to 2.4V. It would be very beneficial if while the

6. References

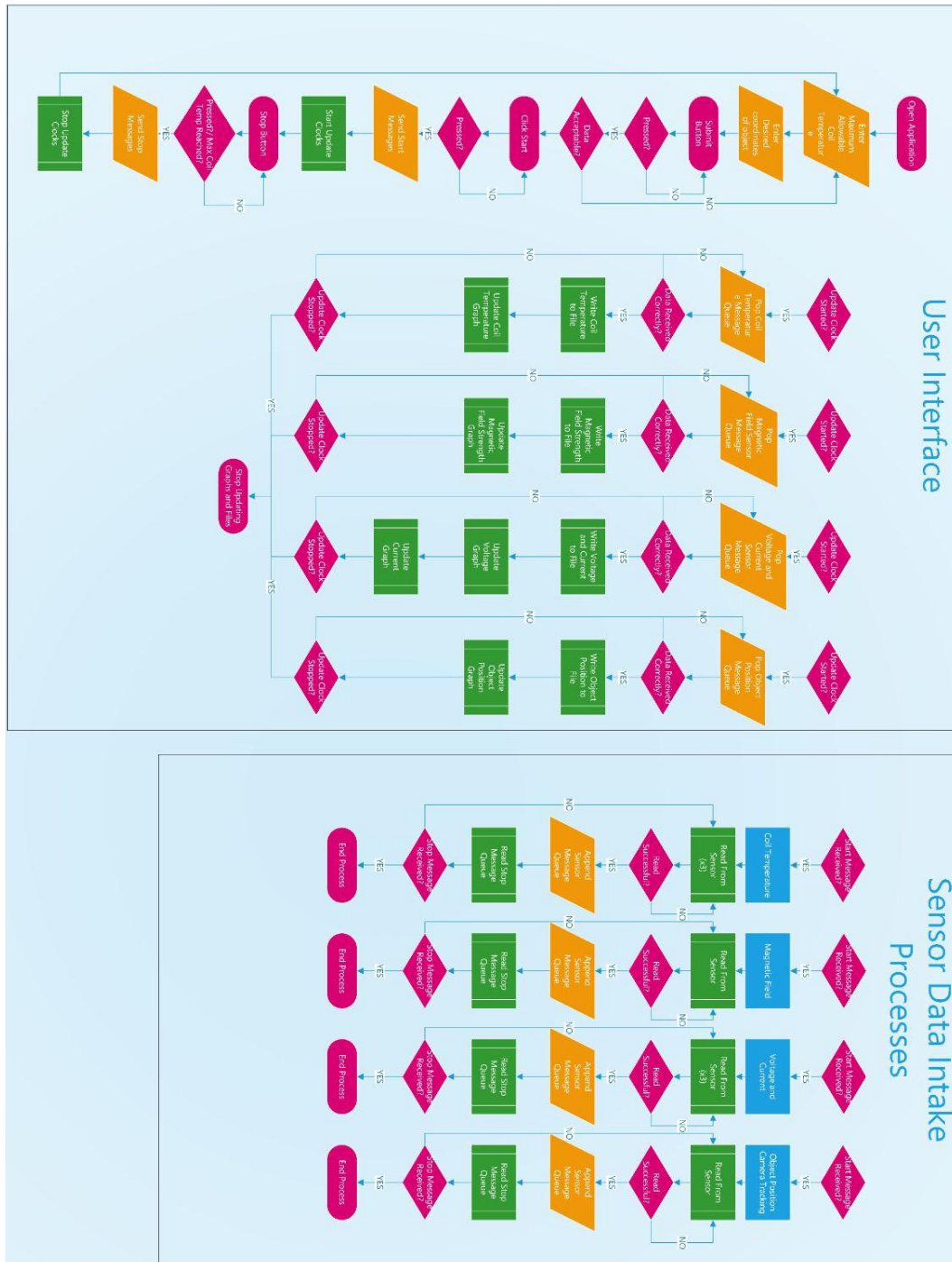
1. George, P.D., Sokolovsky, P. (2023) Micropython, machine library [code library]. <https://docs.micropython.org/en/latest/library/machine.html>
2. George, P.D., Sokolovsky, P. (2023) Micropython, _thread library [code library]. https://docs.micropython.org/en/latest/library/_thread.html
3. Wagner, D. Investigation 4: schematic diagram (January 2023)
4. Duguid, D. discussion on floating references in h-bridge design (March 2023)
5. Pham, L.N., Tabor, G.F., Pourkand, A. et al. Dexterous magnetic manipulation of conductive non-magnetic objects. *Nature* 598, 439–443 (2021). <https://doi.org/10.1038/s41586-021-03966-6>
6. Polymaker Material Comparison Tool [Computer software]. (2023). Retrieved from <https://app.powerbi.com/view?r=eyJrJoiOGlxOTRjM2EtMGVhYS00ZDEwLWJmNTktYTlkYzRIOWY2Nzk2liwidCI6IjUzOTgwYzA1LWI4MWYtNDM2My04OWNiLTU3NzRiMWFiYWYyZCIsImMiOiJFwJFQ%3D%3D>
7. A. J. Petruska and J. J. Abbott, "Omnimagnet: An Omnidirectional Electromagnet for Controlled Dipole-Field Generation," *IEEE Trans. Magnetics*, 50(7):8400810(1-10), 2014. Retrieved from https://www.telerobotics.utah.edu/uploads/Main/Petruska_TMAG14.pdf
8. Blue Sea Systems. (n.d.). Allowable amperage in conductors - wire sizing chart. Retrieved December 1, 2023, from https://www.blueseasystems.com/support/reference/529/Allowable_Amperage_in_Conductors_-_Wire_Sizing_Chart
9. Microsystems, A. (2022, March 17). ACS37800 datasheet - Allegro Microsystems. ACS37800 Datasheet. Retrieved April 11, 2023, from https://www.allegromicro.com/-/media/files/datasheets/acs37800-datasheet.ashx?sc_lang=en&hash=1C7B0351F268B7F35F9A980074E4AA61
10. Eser, A. Y. (2020, August 17). OpenCV camera calibration. Medium. Retrieved April 10, 2023, from <https://aliyasin.eser.medium.com/opencv-camera-calibration-e9a48bdd1844>
11. GeeksforGeeks, G. G. (2023, January 3). Camera Calibration with Python – OpenCV. GeeksforGeeks. Retrieved April 10, 2023, from <https://www.geeksforgeeks.org/camera-calibration-with-python-opencv/>
12. IPC, I. P. C. (2003, May). Generic Standard on Printed Board Design - IPC. Generic Standard on Printed Board Design. Retrieved April 10, 2023, from <https://www.ipc.org/TOC/IPC-2221B.pdf>
13. Maxim Integrated, M. I. (2013). MAX31820 1-Wire Ambient Temperature Sensor . Retrieved April 10, 2023, from <https://www.analog.com/media/en/technical-documentation/data-sheets/MAX31820.pdf>
14. Opencv, O. C. V. (2022, December 28). Opencv/opencv at 4.7.0. GitHub. Retrieved April 10, 2023, from <https://github.com/opencv/opencv/tree/4.7.0>
15. Kivy, K. (2011). KIVY: Cross-platform Python Framework for GUI. Cross-platform Python Framework for GUI apps Development. Retrieved April 10, 2023, from <https://kivy.org/>
16. Pyserial, P. (2021, December). Pyserial/pyserial: Python serial port access library. GitHub. Retrieved April 10, 2023, from <https://github.com/pyserial/pyserial/>
17. Texas Instruments, T. I. (2021, June). TMAG5273 low-power linear 3D Hall-effect sensor with I2C interface ... Low-power linear 3D Hall-effect sensor with I²C interface. Retrieved April 10, 2023, from <https://www.ti.com/lit/ds/symlink/tmag5273.pdf?ts=1624464185137>
18. Mornsun, M. (2022). LM100-20B12_Industrial power supply manufacturer. Mornsun. Retrieved April 11, 2023, from <https://www.mornsun-power.com/html/pdf/LM100-20B12.html>
19. Mornsun, M. (2021). LM25-23B05_industrial power supply manufacturer. Mornsun. Retrieved April 10, 2023, from <https://www.mornsun-power.com/html/pdf/LM25-23B05.html>
20. The Python Software Foundation, T. P. S. F. (2023). Multiprocessing - process-based parallelism. Python documentation. Retrieved April 10, 2023, from <https://docs.python.org/3/library/multiprocessing.html>

7. Appendices

Appendix A: Github Repository

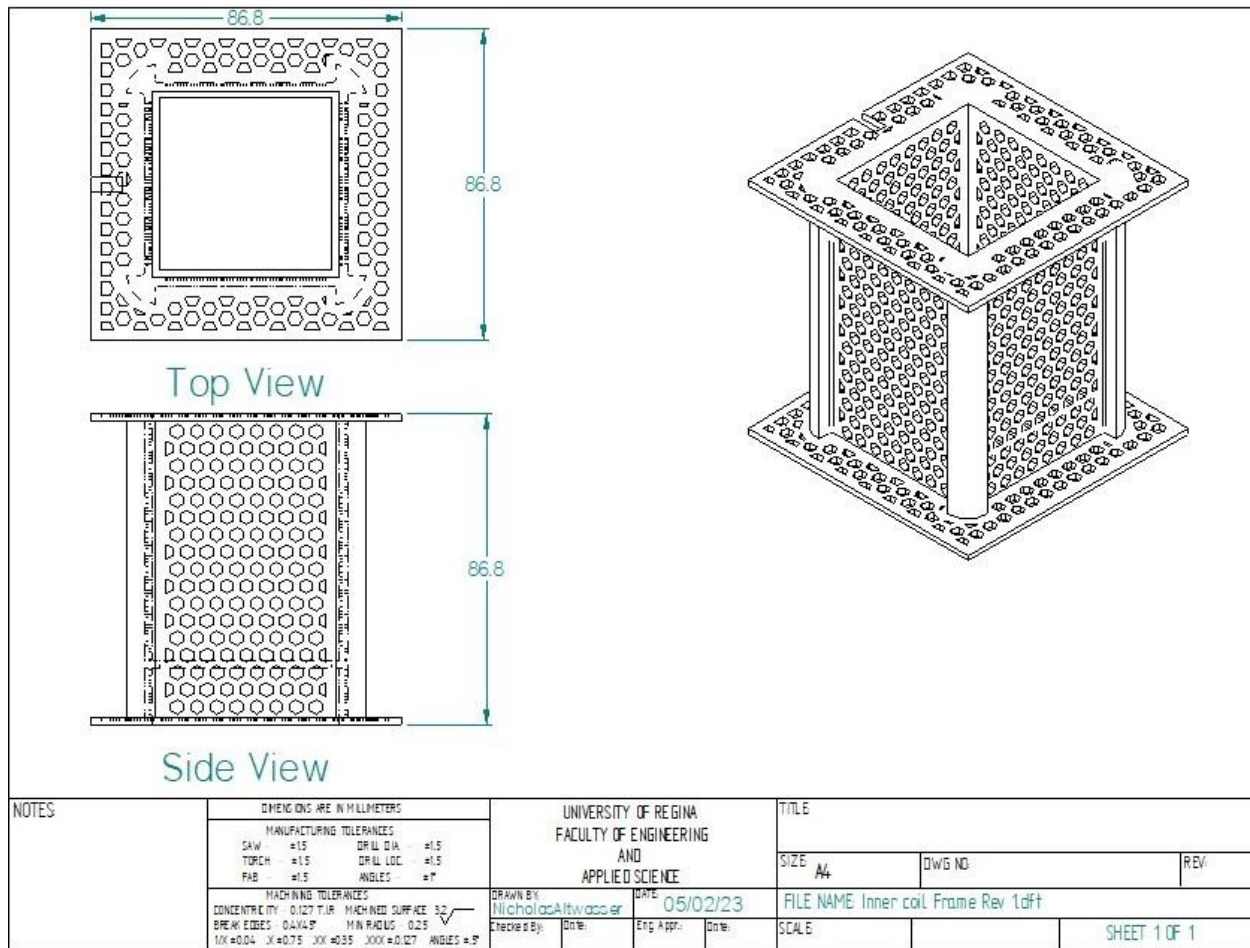
<https://github.com/Palliser7/Enel-Capstone-Project>

Appendix B: Data Logging System Code Block Diagram

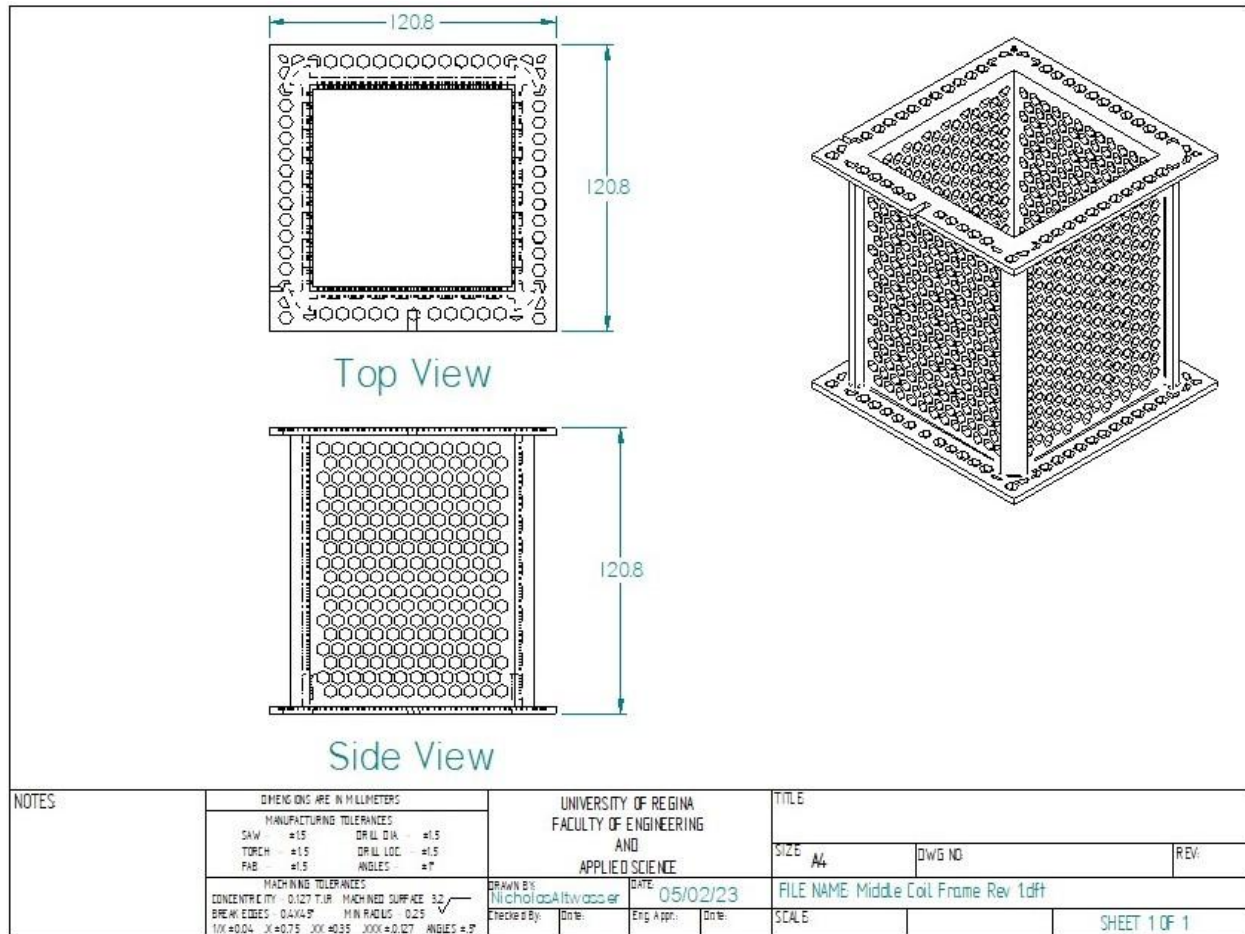


Appendix C: CAD Drawings

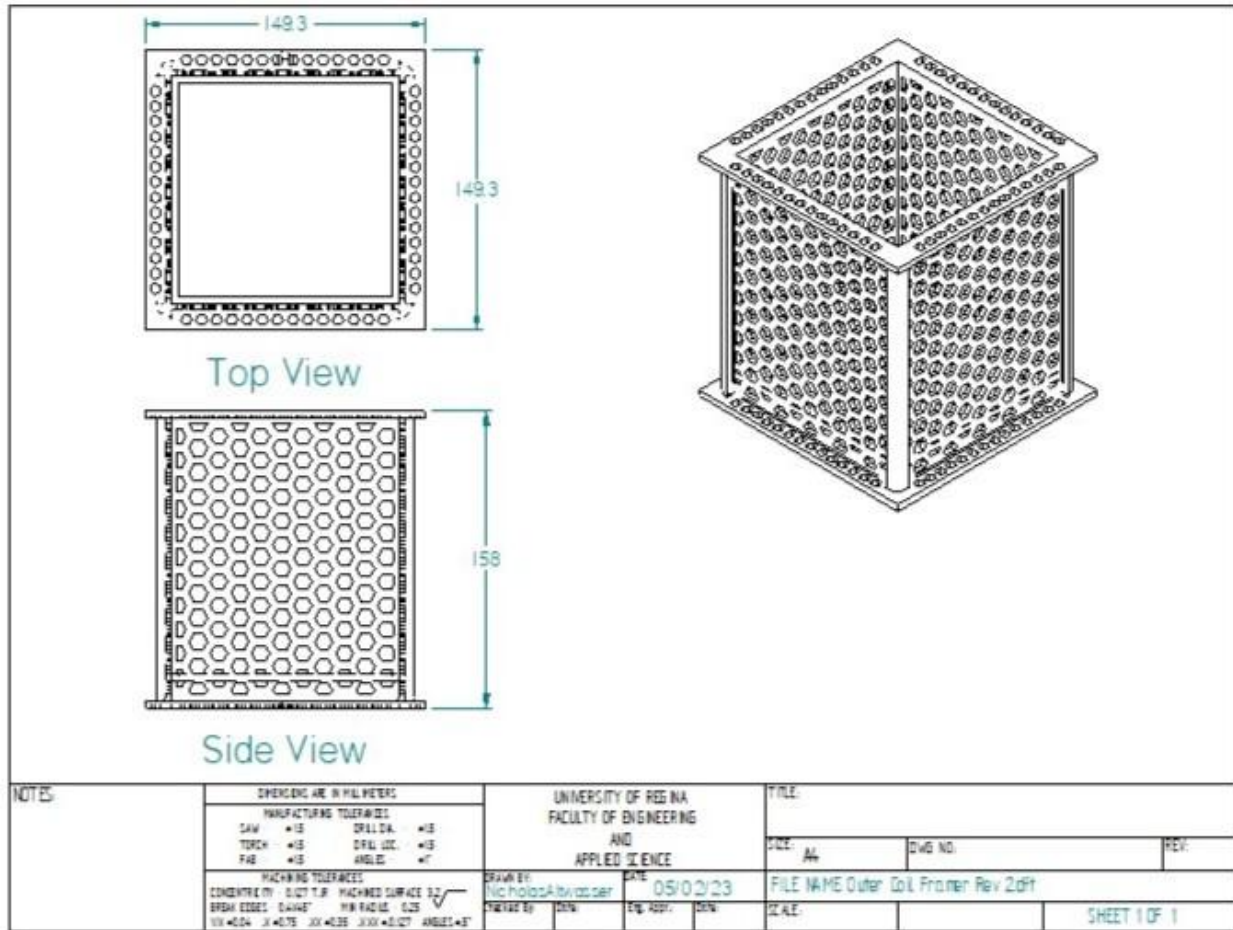
Inner Coil Frame Drawing



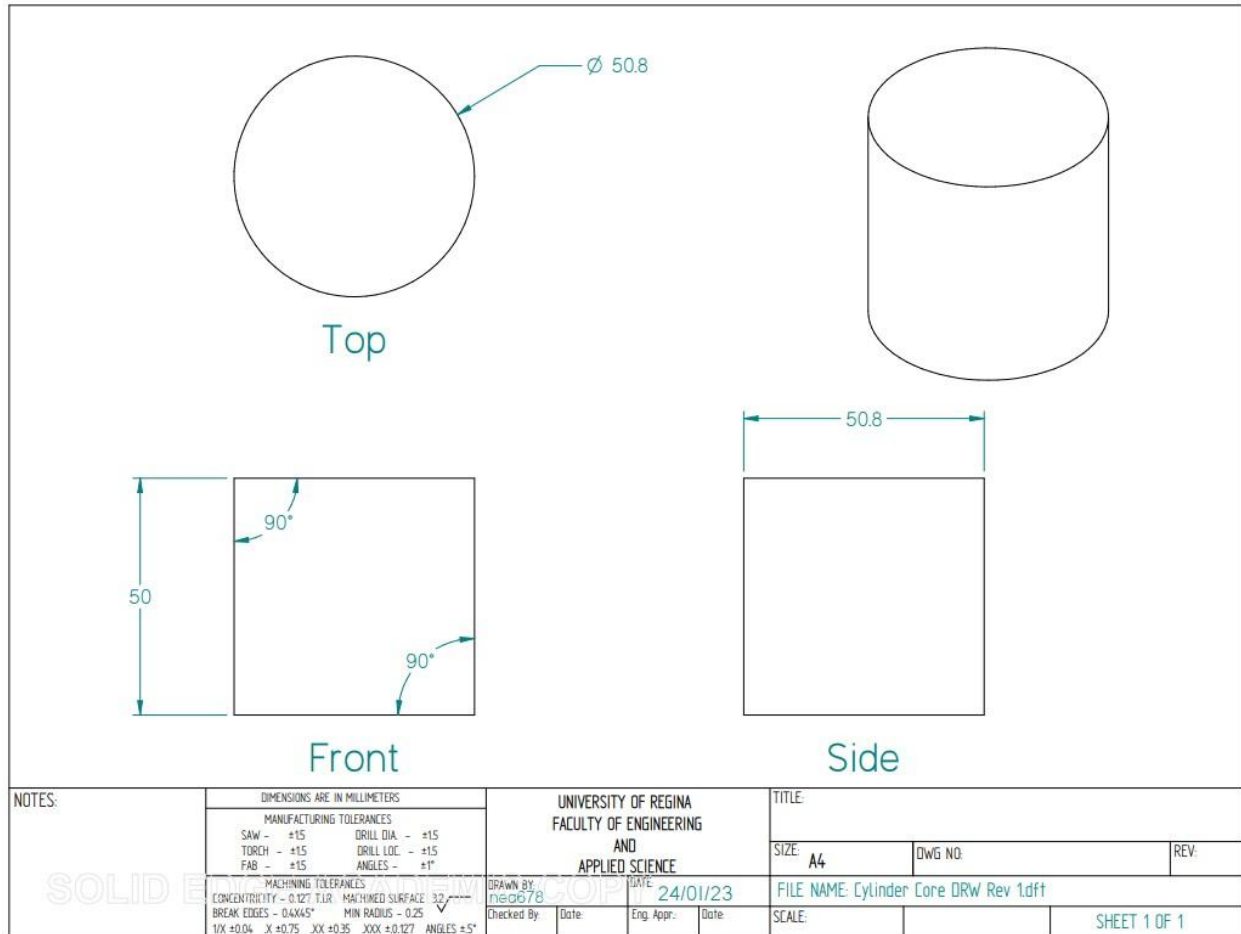
Middle Coil Frame Drawing




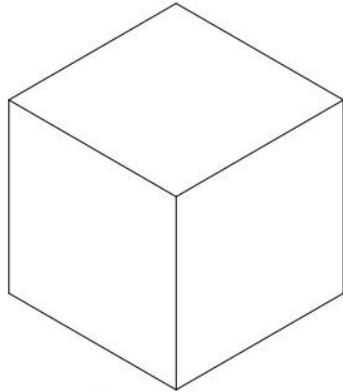
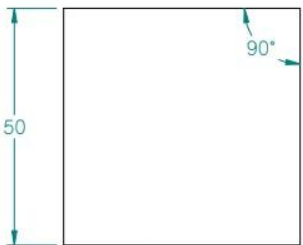
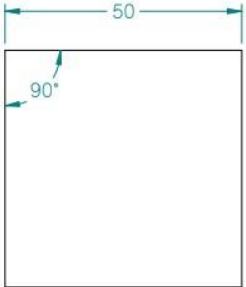
Outer Coil Frame Drawing



Cylindrical Core Drawing

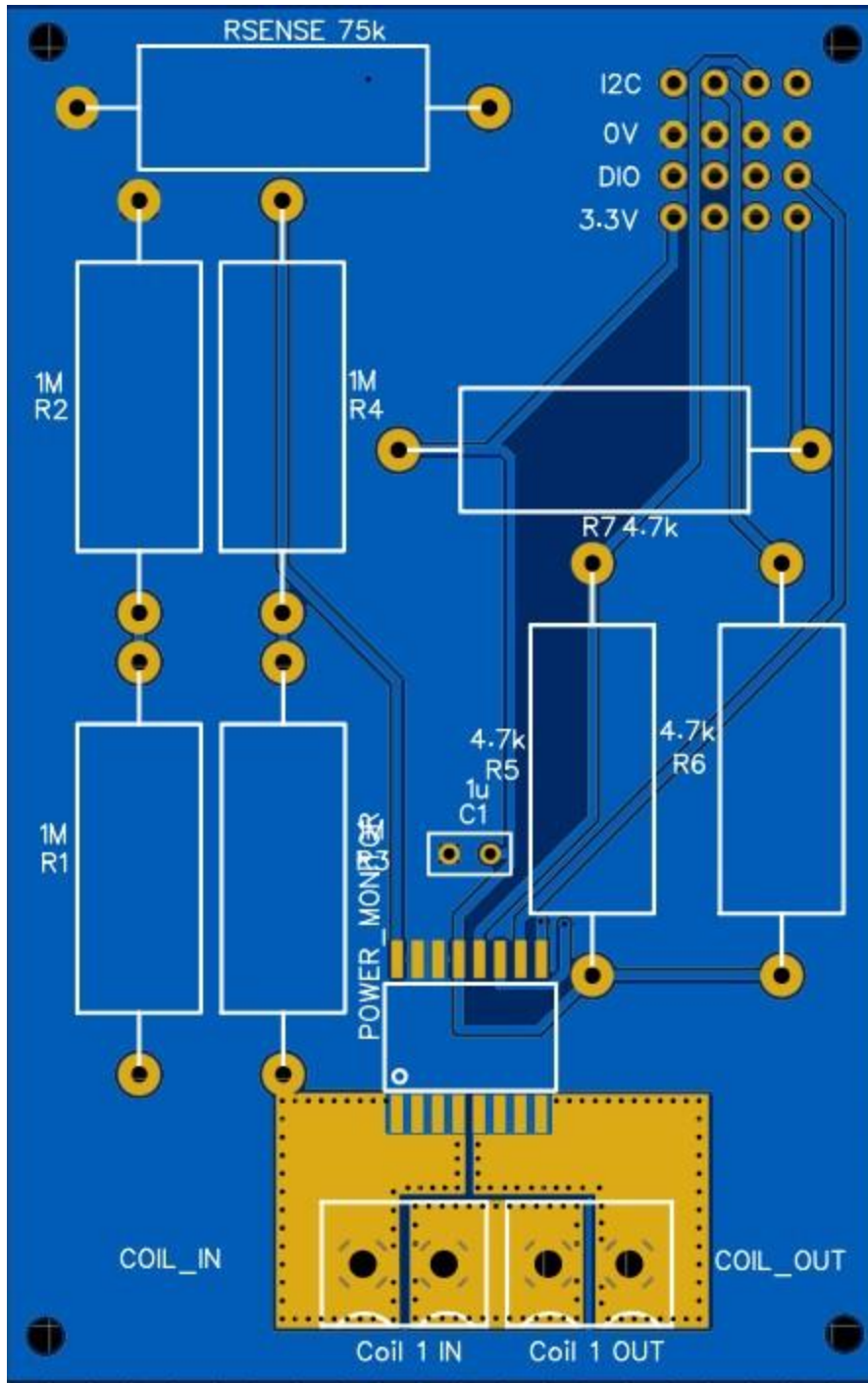


Cube Core Drawing

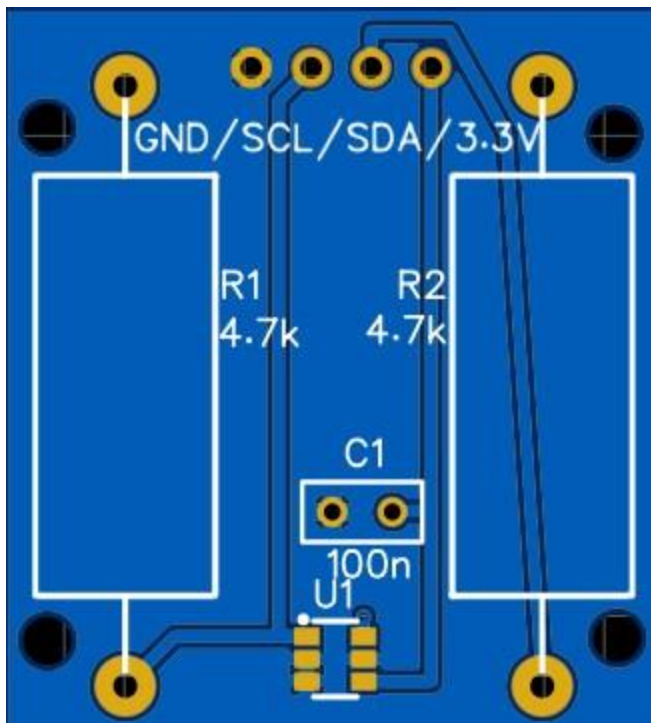
 <p>Top</p>				
 <p>Front</p>		 <p>Side</p>		
NOTES:	DIMENSIONS ARE IN MILLIMETERS MANUFACTURING TOLERANCES SAW - ±15 DRILL DIA. - ±15 TORCH - ±15 DRILL LOC. - ±15 FAB - ±15 ANGLES - ±1°		UNIVERSITY OF REGINA FACULTY OF ENGINEERING AND APPLIED SCIENCE	
	MACHINING TOLERANCES CONCENTRICITY - 0.127 TLR MACHINED SURFACE $\sqrt{3.2}$ BREAK EDGES - 0.4X45° MIN RADIUS - 0.25 10X ±0.04 X ±0.75 XX ±0.35 XXX ±0.127 ANGLES ±5°		TITLE: SIZE: A4 DWG NO: REV:	
	DRAWN BY: nege78 DATE: 24/01/23 FILE NAME: Cube Core DRW Rev 1.dft		SCALE: SHEET 1 OF 1	
	Checked By: Date: Eng. Appr: Date:			

Appendix D: PCB Design:

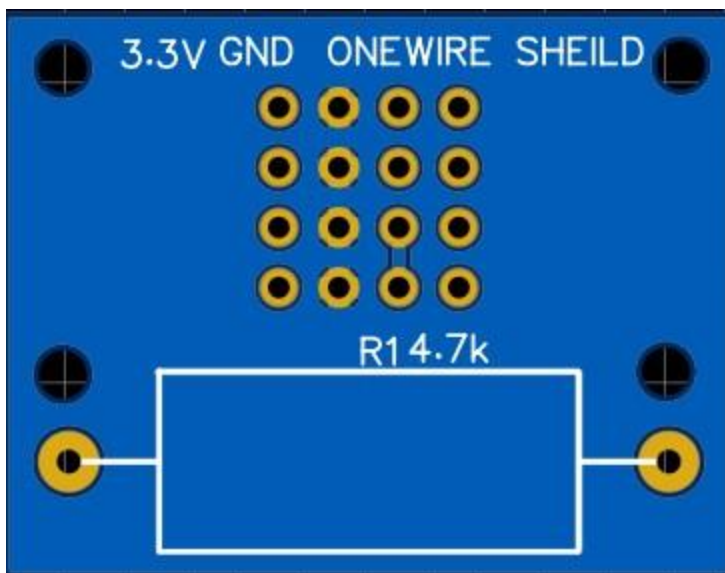
Power Monitoring PCB



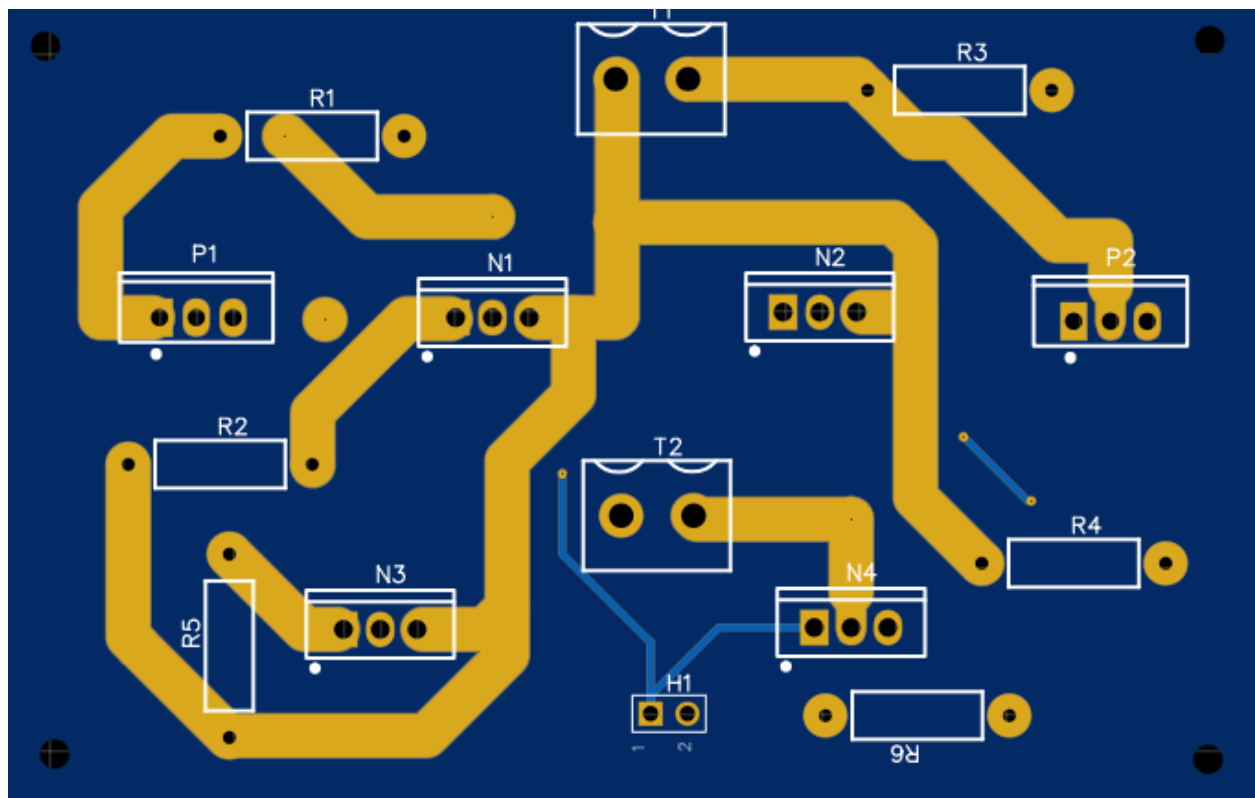
Magnetic Flux Density Sensor PCB



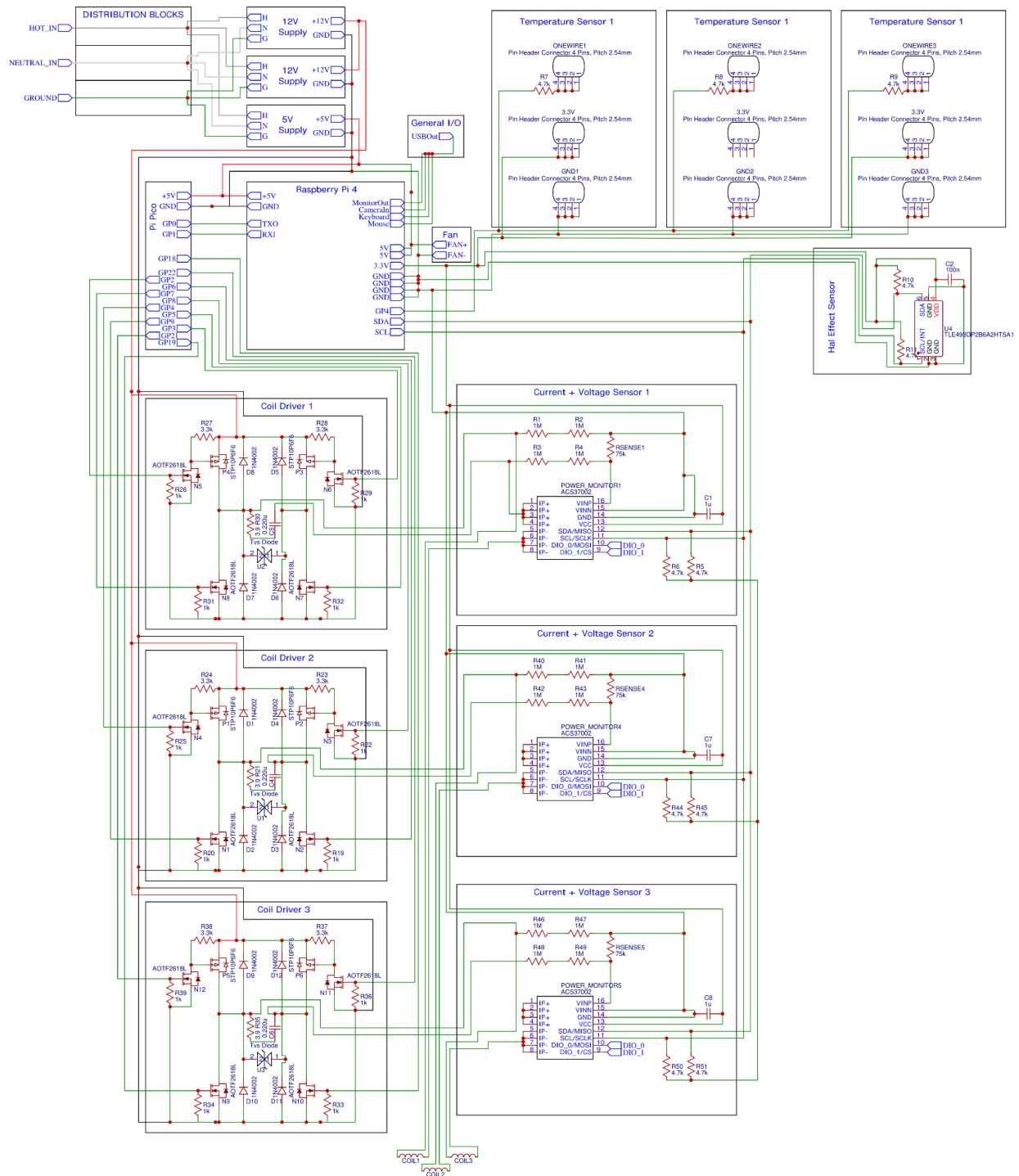
Temperature Sensor PCB



Coil Driver PCB



Full System Schematic



Appendix D: Budget

Full Budget Breakdown

Paid For Agency		Not Paid For NIA		Not Paid For Bryson, No Requests/Notes, Link in Ref Document	
Item	Price	Item/Invoice Name	Price	Item	Location
TEAMC Light Wire	251.91	Digway 1	166.9	Commercial Electric Speaker Boxes Plug (2-Pack)	Home Depot
		Digway 2	132.09	Canon Nikon cord and gpiy ring 3.6 m	Home Depot
		Digway 3	94.01	10 Gauge 25 FT Black Primary Wire	primoskullco
		Digway 4	60.82	Amazon	primoskullco
		Digway 5	16.46	150' 24 in. Self-Healing Cutting Wire	primoskullco
		Digway 6	30.28	120' Gauge Electrical Cord Good by the Foot	primoskullco
		Project Manager	67.27	15A 125V Male Plug	primoskullco
		PC Setup 1	11.5		
		PC Setup 2	46.25		
		Spares	1075.47		
Total (C/O S)	251.91	Total (C/O S)	327.59	Total	147.25
Totals	C/O S	Grand Total (C/O S)	1602.53		
Non-Paid NIA With Invoices	251.91	Budget (C/O S)	2000		
Non-Paid NIA Without Invoices	1075.47	Over/Under (+) (C/O S)	197.47		
Non-Paid Bryson Without Invoices	147.25				